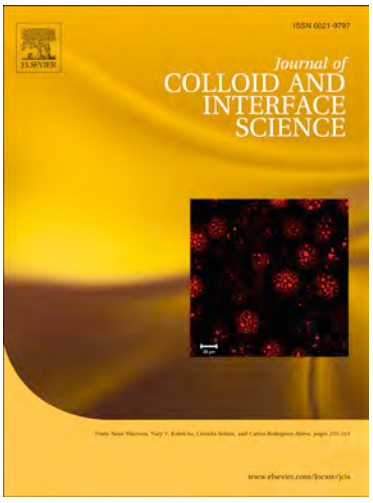

Controlled release of bupivacaine using hybrid thermoresponsive nanoparticles activated via photothermal heating

Teresa Alejo, Vanesa Andreu, Gracia Mendoza, Victor Sebastian, Manuel Arruebo

PII: S0021-9797(18)30363-1
DOI: https://doi.org/10.1016/j.jcis.2018.03.107
Reference: YJCIS 23457

To appear in: *Journal of Colloid and Interface Science*

Received Date: 23 February 2018
Revised Date: 28 March 2018
Accepted Date: 29 March 2018

Please cite this article as: T. Alejo, V. Andreu, G. Mendoza, V. Sebastian, M. Arruebo, Controlled release of bupivacaine using hybrid thermoresponsive nanoparticles activated via photothermal heating, *Journal of Colloid and Interface Science* (2018), doi: https://doi.org/10.1016/j.jcis.2018.03.107

Controlled release of bupivacaine using hybrid thermoresponsive nanoparticles activated via photothermal heating

Teresa Alejo[a,*], *Vanesa Andreu*[a], *Gracia Mendoza*[a], *Victor Sebastian*[a,b], *Manuel Arruebo*[a,b]

[a] Department of Chemical Engineering. Aragon Institute of Nanoscience (INA), University of Zaragoza, Campus Río Ebro - Edificio I+D, C/ Poeta Mariano Esquillor S/N, 50018-Zaragoza, Spain; Aragon Health Research Institute (IIS Aragón), 50009 Zaragoza, Spain.

[b] Networking Research Center on Bioengineering, Biomaterials and Nanomedicine, CIBER-BBN, 28029-Madrid, Spain.

* Corresponding author: Teresa Alejo: teresaal@unizar.es

ABSTRACT

Near-infrared (NIR) responsive nanoparticles are of great interest in the biomedical field as antennas for photothermal therapy and also as triggers for on-demand drug delivery. The present work reports the preparation of hollow gold nanoparticles (HGNPs) with plasmonic absorption in the NIR region covalently bound to a thermoresponsive polymeric shell than can be used as an on-demand drug delivery system for the release of analgesic drugs. The photothermal heating induced by the nanoparticles is able to produce the collapse of the polymeric shell thus generating the release of the local anesthetic bupivacaine in a spatiotemporally controlled way. Those HGNPs contain a 10 wt.% of polymer and present excellent reversible heating under NIR light excitation. Bupivacaine released at physiological temperature (37 ºC) showed a pseudo-zero order release that could be spatiotemporally modified on-demand after applying several pulses of light/temperature above and below the lower critical solution temperature (LCST) of the polymeric shell. Furthermore, the nanomaterials obtained did not displayed detrimental effects on four mammalian cell lines at doses up to 0.2

mg/mL. From the results obtained it can be concluded than this type of hybrid thermoresponsive nanoparticle can be used as an externally activated on-demand drug delivery system.

Keywords: thermoresponsive polymer; phototriggerable; on-demand; plasmonic nanoparticles; anesthetic drug

1. Introduction

Hybrid systems composed of inorganic nanoparticles encapsulated in an organic shell are promising materials that have been recently developed showing unique properties and functions. The functionality of these systems depends on the shape and size of the inorganic core and on the type of organic shell that provides the construct with the surface properties desired for the envisaged application. Moreover, the combination of inorganic nanoparticles and polymeric shells might produce complementary and novel properties that are not found in their individual components. Consequently hybrid nanocomposites composed of metal [1-3], metal oxide [4-6] or non-metal [7-10] nanoparticles have been used for different applications. On-demand drug delivery is required when dosing and timing would produce an improved outcome of the pathology compared to conventional sustained or controlled delivery. This methodology has the advantage of controlling local dosing so that the drug is released at a specific time and with a chosen dose, moreover the dose supplied can be modified according to the patient needs. For instance, in the treatment of chronic pain or hormonal disorders the doses required can be supplied depending on the disease progresses. Pulsatile release of drugs can also be useful in the treatment of diabetes through on demand insulin delivery [11]. Nanomaterials have great potential as on-demand drug delivery systems as they allow reduced toxicity, side effects and provide with a more rational usage of the carried drug reducing under or overdose. Different external triggers can be used to activate the release including physical stimuli (e.g., light, temperature, alternating magnetic fields, ultrasounds, etc.) and biochemical stimuli (e.g., acidic environment, redox potential, presence of specific moieties, etc.). In this regard, proteins were efficiently loaded into pH and reductive environment responsive nanosized polymersomes prepared from polyethylene glycol (PEG)-based block copolymers. The release of proteins was triggered specifically at endosomal pH

(i.e., pH 6) or under the reductive conditions of cytosol (10 mM dithiothreitol), so the amount released was significantly higher than that reached at physiological conditions (pH 7.4 and 37 ºC) [12]. Micelles composed of dendrimers and boronic acid or catechol at the interfase were developed for the release of the chemotherapeutic drug paclitaxel upon the addition of mannitol or under acidic conditions (i.e., pH 5) [13]. This system is also sensitive to oxidizing agents being interesting for oxidation-assisted triggered release [14]. In addition, hybrid nanomaterials triggered by temperature have been widely used in biomedicine, particularly in cancer treatment [7, 15-17]. Magnetic nanoparticles combined with thermoresponsive polymers allow to deliver heat promoting drug desorption locally under the presence of an alternating magnetic field to be potentially used not only in triggered drug delivery but also in hyperthermal therapy [15, 16, 18].

Thermoresponsive copolymers derived from oligo (ethylene glycol) methacrylate with reversible transition above and below their LCST are biocompatible materials suitable as injectable drug delivery systems [19-21]. Another transition-reversible thermosensitive polymer, such as poly(N-isopropylacrylamide) (PNIPAM), has been widely used in different biomedical applications including triggered drug delivery [22], biosensing [23], cell culturing [24], encapsulation [25], and tissue engineering [26]. However, it presents some disadvantages, such as lower biocompatibility and hysteresis in its phase transition, compared to OEGMA-based copolymers [27-29]. Lutz et al. [30] described the preparation of thermoresponsive copolymers based on OEGMA using atom transfer radical polymerization (ATRP). They reported the ATRP of OEGMA and MEO_2MA copolymers initiated by methyl 2-bromopropionate (MBP) using a chloride-based CuCl/bipy catalyst, leading to a good control in the polymerization. These polymers are soluble in water and undergo a transition to water-insoluble materials above their LCST. This transition temperature can be tuned by changing the oligo (ethylene glycol) methyl ether methacrylate (OEGMA) and di (ethylene glycol) methyl ether methacrylate (MEO_2MA) monomer ratio [30]. This phenomenon has been used for the remote-controlled drug delivery [31-33]. The release of encapsulated drugs can be triggered in response to a temperature driven stimuli induced by irradiation of light at the extinction peak of the nanomaterial inorganic core. Surface plasmonic resonance in nanoparticles induces localized heating within the thermoresponsive shell. When the temperature rises above the LCST of the polymer, the polymer shell collapses resulting in an on-demand burst release of drugs

trapped on it as opposed to a diffusion-controlled release. Compared to visible light, irradiation with NIR light allows deeper tissue penetration and diminishes tissue injuries potentially incurred in the patient [34]. Consequently, NIR activated drug delivery systems have been previously used to promote controlled delivery of drugs entrapped into thermoresponsive polymers [35, 36]. For example, Zhang et al. have reported the release of doxorubicin in a controlled manner from mesoporous-silica-coated gold nanorods modified with PNIPAM after activation upon NIR light irradiation [35]. However, to the best of our knowledge, the triggered release of an encapsulated drug from plasmonic nanoparticles decorated with a POEGMA-based shell has not been previously reported.

The spatial and temporal controlled-release of drugs for improved pain management is a major challenge for its adequate treatment. Bupivacaine hydrochloride is a local anesthetic that blocks the generation and conduction of nerve impulses. It is widely used in epidural infusions to provide post-operative analgesia [37, 38], and for Caesarean sections [39]. Bupivacaine hydrochloride has been demonstrated to have long-term stability [40, 41], thus it has been previously chosen as a model drug to be incorporated within nanoparticulate carriers for the treatment of chronic pain. In a preceding study, Dihn et al. [42] incorporated bupivacaine in poly(lactic-co-glycolic acid) (PLGA) NPs within collagen-based injectable composite hydrogels in which the release could be controlled by changing the ratio of the different monomeric components. Microparticles composed of PLGA were also applied for controlled bupivacaine release showing no cytotoxicity or proinflammatory effects [43]. PNIPAM-based nanogels exhibited ionic affinity for binding bupivacaine which produced an effective drug loading [44] and achieved nerve block durations of up to 9h [45]. Herein, HGNPs with NIR optical properties are functionalized with a thermoresponsive OEGMA-based copolymer shell to be used as drug carriers for the controlled delivery of an entrapped drug under external stimuli. HGNPs act as NIR light absorbing materials suitable for photothermal triggered drug delivery. The loading and the release profiles of the local anesthetic bupivacaine were determined to study the nanoparticles efficiency and the effect of the light/temperature stimuli in the release process.

2. Experimental Section

2.1. Materials and methods

Di(ethylene glycol) methyl ether methacrylate (MEO_2MA) (95%), oligo(ethylene glycol) methyl ether methacrylate (OEGMA) (Mn 500 g mol^{-1}), 2,2′bipyridyl (bipy) (98%), bis[2-(2-bromoisobutyryloxy)undecyl] disulfide (97%), anhydrous ethanol (Panreac, 0.02% water), cobalt chloride hexahydrate (ACS reagent grade), sodium citrate tribasic dihydrate (≥98%), poly(vinylpyrrolidone) (PVP, Mw = 55000 Da), sodium borohydride (≥99%), gold(III) chloride hydrate (~50% Au basis), ammonium persulfate (APS) (>98%), ethylene glycol dimethacrylate (EGDMA) (>98%), sodium dodecyl sulfate (SDS) (>98%) and bupivacaine hydrochloride monohydrate (≥99%) were purchased from Sigma-Aldrich. All of these chemicals were used as received. Copper(I) chloride (Sigma Aldrich, 97%) was washed with glacial acetic acid and ethanol and dried to remove oxidized species before use.

Proton nuclear magnetic resonance (^{1}H-NMR) spectroscopy was carried out on a Bruker AV-400 spectrometer operating at 400 MHz using $CDCl_3$ as solvent. Fourier transform infrared (FTIR) spectroscopy analysis was performed on a Bruker Vertex 70 FTIR spectrometer equipped with a deuterated triglycine sulfate (DTGS) detector and a Golden Gate diamond attenuated total reflectance (ATR) accessory. The scans were performed in the wavelength range of 4000-400 cm^{-1}. Thermogravimetric analysis (TGA; Mettler Toledo TGA/STDA 851e) was carried out in a temperature range between 30 and 800 ºC using a heating rate of 10 ºC/min under nitrogen atmosphere.

The LCST of the polymer solutions (3 mg mL^{-1}) in deionized water was determined from the optical transmittance measurements at 670 nm as a function of temperature using a Varian Cary® 50 UV-Visible spectrometer (Agilent Technologies, USA) equipped with an optic fiber dip probe. UV-vis spectra were recorded using a Jasco V670 spectrophotometer to evaluate the characteristic HGNPs surface plasmon resonance band in the NIR region of the electromagnetic spectrum. Dynamic light scattering (DLS) measurements and analysis were performed on a Brookhaven 90Plus particle size analyzer with a detection angle of 90º. Measurements were taken at 25 ± 0.1 ºC. Zeta potential of the nanoparticles was measured in the same equipment using the ZetaPALS software in 1 mM KCl aqueous solution at a pH = 6 and 25 ± 0.1 ºC.

Transmission electron microscopy (TEM) images were recorded on a T20-FEI Tecnai thermoionic microscope operated at an acceleration voltage of 200 kV. Aberration corrected scanning transmission electron microscopy (Cs-corrected STEM) images were acquired using a high angle annular dark field detector (HAADF) in a FEI XFEG TITAN electron microscope operated at 300 kV equipped with a CETCOR Cs-

probe corrector from CEOS. Elemental analysis was carried out with an EDS (EDAX) detector, which allows performing EDS experiments in the scanning mode. Samples were dropped in carbon coated copper grids, dried at room temperature and stained with a negative staining agent (phosphotungstic acid) when necessary to improve the contrast of the thermoresponsive polymeric shell.

Nanoparticle irradiation was performed using a 808nm-laser diode (model MDL-III-808-2W, Changchun New Industries Optoelectronics Technology Co., Ltd., Changchun, P.R. China). Samples were irradiated as dispersions in water at a concentration of 1.6 mg/mL using a laser irradiance of 6.5 W/cm^2.

2.2. Synthetic procedures

2.2.1. Synthesis of disulfide-P(MEO$_2$MA-co-OEGMA$_{500}$)

The thermoresponsive disulfide-P(MEO$_2$MA-co-OEGMA$_{500}$) polymer was prepared by ATRP using a CuCl/bipy complex as catalyst. The synthesis was performed in ethanol at 60 ºC using the disulfide-functionalized bis[2-(2-bromoisobutyryloxy)undecyl] disulfide initiator, adapted from the method described by Lutz and Hoth [30] using a molar ratio [monomers]$_0$/[Initiator]$_0$/[CuCl]$_0$/[bipy]$_0$ = 100/1/1/2. The MEO$_2$MA / OEGMA$_{500}$ monomer ratio used was (88/12) to adjust the LCST within the physiological temperature [46]. The final product was purified by passing the ethanolic solution containing the resulting polymer through a silica gel (60-120 mesh) column. Then, the solvent was further removed using a rotary evaporator, and the polymer was dispersed in water and dialyzed (molecular weight cut-off 14000 Da) against water/ethanol mixtures for at least 72 h to ensure the removal of the non-reacted monomers. Finally, water was removed by lyophilization to yield the polymer as a colorless oil.

2.2.2. Synthesis of hollow gold nanoparticles (HGNPs)

The synthesis of HGNPs was performed using previously reported methods [47, 48]. Briefly, in a two-necked round-bottom flask, 400 mL of deionized water was combined with 400 μL of 0.35 M cobalt chloride hexahydrate and 1.6 mL of 0.1 M sodium citrate trihydrate. The solution was deoxygenated by bubbling it with argon gas for 45 minutes with no magnetic stirring. To that solution, 2 mL of 1 wt.% solution of poly (vinylpyrrolidone) and 400 μL of 1.0 M sodium borohydride was added under

magnetic stirring, and the solution turned to brown indicating the formation of cobalt nanoparticles. The cobalt nanoparticle dispersion was further stirred under argon flux during 15 minutes. Afterwards, 380 mL of the cobalt nanoparticle dispersion was added to a solution containing 120 mL of deionized water and 180 μL of 0.1 M gold (III) chloride hydrate under stirring. The final dispersion was stirred at ambient conditions during 30 minutes to complete the oxidation of the residual cobalt, thus the dispersion turned from brown to green indicating the presence of HGNPs. The resulting dispersion was centrifuged at 13000 rpm several times to remove potential unreacted reagents.

2.2.3. Grafting of disulfide-P(MEO_2MA-co-$OEGMA_{500}$) polymer to HGNPs

HGNPs were coated with the disulfide-functionalized P(MEO_2MA-co-$OEGMA_{500}$) polymer. The strong interaction between the disulfide end-group of the polymer and the gold surface of the nanoparticles allows the covalent and electrostatic attachment of the polymer to the nanoparticles [49, 50]. A dispersion of the polymer and the HGNPs in a weight ratio (1:1) was stirred during 3 h at room temperature. Afterwards the excess of polymer was washed by centrifugation with water (3 times, 13000 rpm).

2.2.4. Synthesis of HGNPs@P(MEO_2MA-co-$OEGMA_{500}$) core-shell nanogels

HGNPs@P(MEO_2MA-co-$OEGMA_{500}$) were used as starting material to tailor a thick nanogel shell on the surface of the nanoparticles. The synthesis was done using the nanoprecipitation polymerization method based on the protocol reported by Guarrotxena et al. [51] Briefly, a typical synthesis was depicted as follows: in a Schlenk tube, 4.5 mg of as-prepared P(MEO_2MA-co-$OEGMA_{500}$) capped HGNPs, 0.546 mmol of MEO_2MA monomer, 0.0745 mmol of $OEGMA_{500}$ monomer, 0.0185 mmol of EGDMA cross linker and $5.2x10^{-3}$ mmol of SDS surfactant dissolved in 9 mL of deionized water were purged with argon under stirring during 30 min. The [MEO_2MA]/[$OEGMA_{500}$] monomer molar ratio used was 88/12, to maintain the LCST in the physiological range [46]. After purging, the solution was heated to 65 ºC, and the polymerization was initiated by the addition of APS (450 μL, 0.035 M). As the nanoprecipitation polymerization starts, the transparent solution became cloudy. The polymerization was carried out during 2 h and after, the obtained nanoparticles were centrifuged and washed with water three times (2000 rpm, 10 min) to remove unreacted reagents.

2.3. Cell culture and biological studies

The cytocompatibility of the HGNPs@P(MEO_2MA-co-$OEGMA_{500}$) and HGNPs@P(MEO_2MA-co-$OEGMA_{500}$) loaded with bupivacaine was evaluated at different levels regarding metabolism, cell membrane (induction of apoptosis and/or necrosis) and cell nucleus (distribution of cell-cycle phases). These studies were developed in mouse mesenchymal stem cells (mMSCs) and in human glioblastoma cells (U251MG), both kindly gifted by Dr. Pilar Martín-Duque, as well as in human dermal fibroblasts (Lonza, Belgium) and in THP1 human macrophages (American Type Culture Collection, US).

Fibroblasts and U251MG cells were grown in DMEM high glucose (Biowest, France) containing 2 mM L-glutamine and supplemented with 10% v/v fetal bovine serum (Gibco, UK) and 1% penicillin-streptomycin-amphotericin B (Biowest, France), while mMSCs were cultured in DMEM-F12 (Biowest, France) supplemented with 2 mM L-glutamine (Biowest, France), 10% v/v fetal bovine serum (Gibco, UK) and 1% penicillin-streptomycin- amphotericin B (Biowest, France). Monocytes were cultured in RPMI 1640 (Biowest, France) also containing 2 mM L-glutamine and supplemented with 10% v/v fetal bovine serum (Gibco, UK), 1% HEPES, 0.1% 2-mercaptoethanol 50 mM, 1% non-essential aminoacids, 1% sodium pyruvate 100 mM and 1% penicillin-streptomycin-amphotericin B (Biowest, France). Macrophages were obtained by the *in vitro* differentiation of monocytes through the addition of 1 μM phorbol 12-myristate 13-acetate (Sigma Aldrich, US) to the cell culture medium for 72 h. All cell types were cultured at 37 ºC and 5% CO_2, except for mMSCs (hypoxia conditions, 3% O_2).

2.3.1. Cell viability assay

Blue Cell Viability assay (Abnova, Taiwan), which is based on the reduction of a dye to a fluorescent compound mediated by metabolically active cells, was used to determine the effects of our hybrid thermoresponsive nanoparticles on cell metabolism after incubation (0.02- 2 mg/mL) for 24 h. Then, the reagent was added to the cells (10%) and incubated for 4 h (37 ºC, 5% CO_2). After incubation, fluorescence was read (535/590 nm ex/em) in a Synergy HT Microplate Reader (Biotek, US) and viability was calculated by interpolation of the emission data displayed by the treated samples and the control ones (untreated samples = 100% viability).

2.3.2. Evaluation of early and late cell apoptosis and necrosis

In order to evaluate the influence of the nanoparticles in the physiological state of different cell lines (U251MG, Fibroblasts, mMSCs and THP1 macrophages), a quantitative analysis of cell death by apoptosis and necrosis was carried out using a commercial kit (Annexin V FITC kit, Immunostep) according to the manufacturer's instructions. Briefly, cells were treated with nanoparticles (0.2 mg/mL, subcytotoxic concentration obtained from the Blue Cell Viability assay) for 24 h at 37° C and 5% CO_2. After nanoparticle exposure, cells were washed twice with PBS and harvested by centrifugation (1500 rpm, 5 min). Then, cells were resuspended in PBS at final concentration of 10^6 cells/mL. Subsequently, cells were centrifuged at 1200 rpm for 5 min and the pellet was resuspended in 100 µl of Annexin-binding buffer. Then, 50 µl of this cell suspension was stained with Annexin V-FITC and propidium iodide for 15 min at room temperature in the dark. After incubation, 150 µl Annexin-binding buffer was added to each sample. Samples were immediately analyzed via flow cytometry in a FACSARIA BD equipment and the percentages of alive, apoptotic and necrotic cells were calculated using the FACSDIVA BD software (Cell Separation and Cytometry Unit, CIBA, IIS Aragon, Spain).

2.3.3. Cell Cycle analysis

Cell cycle analysis was carried out by flow cytometry using propidium iodide DNA staining. For that, cells exposed to 0.2 mg/mL nanoparticles for 24 h were collected, fixed with 70% ice-cold ethanol and stored at 4 ºC for 24 h. Cells were then centrifuged, washed in PBS and treated with a solution containing RNase A (100 µg/mL; Sigma-Aldrich) and propidium iodide (50 µg/mL; Sigma-Aldrich). After an incubation period of 30 min at room temperature in the dark, samples were analyzed in a Gallios flow cytometer.

3. Results and discussion

3.1. Characterization of the polymer

The PEGylation of nanoparticles is widely used in biomedical applications as PEG is non-toxic and acts as dispersing agent reducing protein adsorption and the fast

clearance by the mononuclear phagocyte system. Here, the disulfide-P(MEO_2MA-co-$OEGMA_{500}$) copolymer coated on the surface of the HGNPs contributes to achieve water dispersity and enhances the core-metal biocompatibility. Moreover, the polymer provides with a thermoresponsive behavior to the Au-based nanoparticles, to be used as thermally-responsive drug delivery systems. The LCST of the synthesized polymer was defined as the temperature at which 50% of the initial transmittance and it was reached [52] by adjusting during the ATRP the molar ratio of the monomers in the final structure. In Fig. 1a the polymer shows a LCST of 41.5 ºC with an OEGMA molar content of 12%. The transmittance curve presented a sharp decrease, which is consistent with a monodisperse distribution of molecular weights in the polymer. This coil-globule transition was tuned above the physiological temperature to a value (41.5 ºC) that could be easily reached thanks to the photothermal heating produced by the HGNP absorption of light in the NIR region. The structure of the disulfide-P(MEO_2MA-co-$OEGMA_{500}$) was corroborated by ^{1}H-NMR spectroscopy, shown by the new signal at 4.1 ppm characteristic of the polymer formation, and the absence of vinyl protons characteristic of the free monomers (5.57 and 6.13 ppm) after purification (Fig. 1b). Fig. 1b shows the principal resonance peaks of the disulfide-terminated polymer obtained. The disulfide end-functionalized polymer is characterized by the following peaks: the ones present at 0.9-1.5 ppm which correspond to the protons of the (-C-(CH_2)$_9$-C-) group of the initiator. The peaks at 4.1, 3.5-3.7 and 3.4 ppm correspond to the main chain protons of the chemical groups (CH_2-CH_2-O), (-CH_2-O-) and (-OCH_3), respectively, and peaks at 1.7-2 and 0.85 ppm are related to the first and second protons of (-CH_2C(CH_3)), respectively [53]. The FTIR spectra of the disulfide-P(MEO_2MA-co-$OEGMA_{500}$) polymer depicted in Fig. 1c showed the characteristic band at 2880 cm^{-1} attributed to C-H stretching vibrations [54]. The peak at 1720 cm^{-1} was assigned to the stretching vibration of C=O groups in the polymer, and the broad band at 1109 cm^{-1} corresponds to C-O-C stretching vibrations [55]. ^{1}H-NMR and FTIR signals in Fig. 1 confirmed that the disulfide-P(MEO_2MA-co-$OEGMA_{500}$) copolymer was obtained. These disulfide groups were used to covalently bind the resulting themoresponsive polymer to gold surfaces via electrostatic and covalent coupling [56].

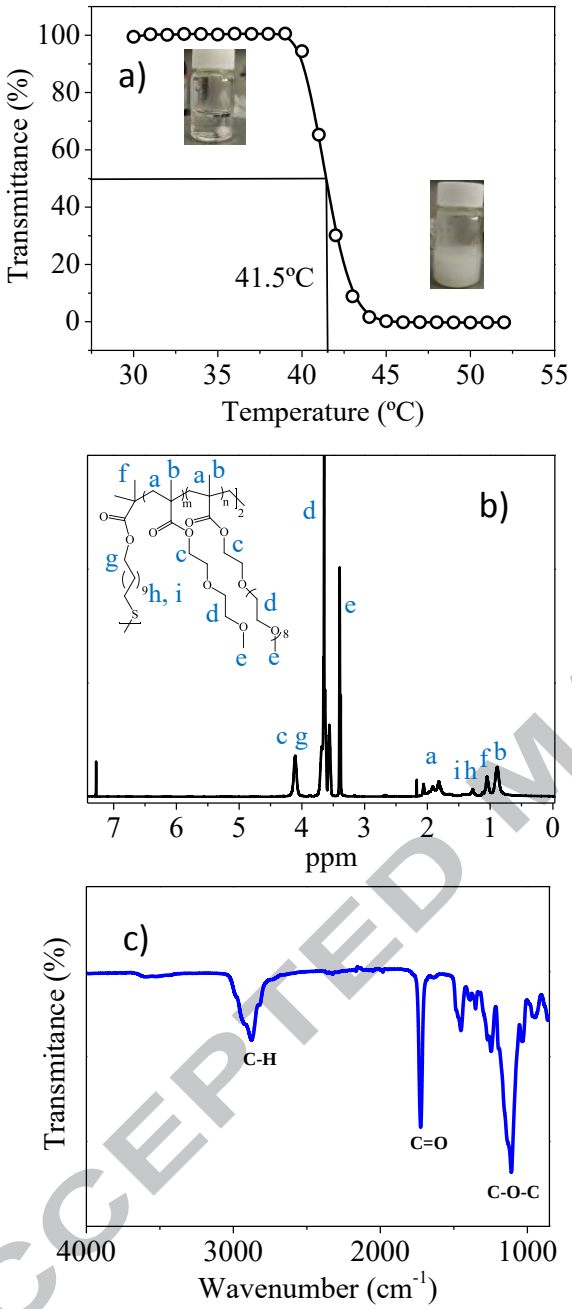

Fig. 1. (a) Transmittance at 670 nm versus temperature for 3 mg/mL disulfide-P(MEO_2MA-co-$OEGMA_{500}$) polymer solution. (b) ^1H NMR spectra of disulfide-P(MEO_2MA-co-$OEGMA_{500}$) copolymer. (c) FTIR of disulfide-P(MEO_2MA-co-$OEGMA_{500}$) copolymer. The LCST was set at 41.5 ºC with a MEO_2MA/$OEGMA_{500}$ ratio of 88:12.

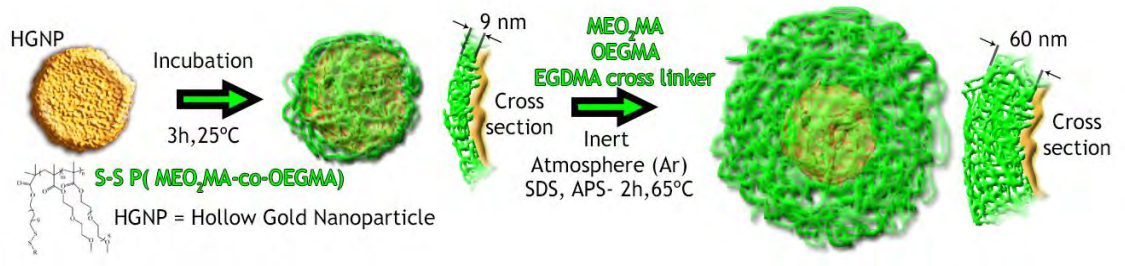

Scheme 1. Synthetic route of HGNPs@P(MEO_2MA-co-$OEGMA_{500}$) monolayer and HGNPs@P(MEO_2MA-co-$OEGMA_{500}$) nanogel.

3.2. Preparation of hybrid HGNPs@P(MEO_2MA-co-$OEGMA_{500}$) core-shell nanoparticles

Scheme 1 represents the synthetic route for the preparation of HGNPs@P(MEO_2MA-co-$OEGMA_{500}$) and HGNPs@P(MEO_2MA-co-$OEGMA_{500}$) nanogels. As-prepared HGNPs were functionalized with the copolymer P(MEO_2MA-co-$OEGMA_{500}$) through the interaction with the disulfide end group of the polymer. Afterwards, HGNPs coated with P(MEO_2MA-co-$OEGMA_{500}$) were used as starting materials for the synthesis of nanogel-composed shells grown onto the nanoparticle surface using the nanoprecipitation polymerization method described above (Scheme 1). Fig. 2a shows TEM images of the resulting HGNPs@P(MEO_2MA-co-$OEGMA_{500}$) after staining with phosphotungstic acid salt to show the thickness (i.e., 9 nm) of the polymeric shell. TEM images revealed the presence of monodisperse nanoparticles of approx. 40 nm in diameter. In Fig. 2b STEM-HAADF images showed a stained sample to identify the location of Au and W atoms by Z–contrast, where W atoms represented the polymeric shell due to the dye used [57]. The polycrystalline structure of the metal nanoparticles is observed in images Fig. 2c-e, where the hollow structure is described in detail. TEM and STEM-HAADF images of HGNPs@P(MEO_2MA-co-$OEGMA_{500}$) nanogels are presented in Fig. 2g-h. The core-shell nanogels are spheroidal in shape with single gold cores homogeneously encapsulated in the nanogel shell. The overall average particle diameter was 206.5 ± 49.3 nm (N=15) with a nanogel shell thickness of ≈ 60 nm. The EDS analysis (Fig. 2f,i) showed the presence of atoms of Au, C and O (and Cu due to the copper grid used). Co atoms were not detected indicating a successful galvanic replacement of Co by Au during the formation of the HGNPs.

Between these two types of hybrid core-shell nanoparticles we selected HGNPs functionalized with the thin polymeric shell monolayer, referred to as

HGNPs@P(MEO_2MA-co-$OEGMA_{500}$) hereafter, for the bupivacaine loading and release studies. The average hydrodynamic diameter of HGNPs@P(MEO_2MA-co-$OEGMA_{500}$) determined by DLS was 65 nm with a polydispersity index of 0.2 which is consistent with the results retrieved from the TEM images.

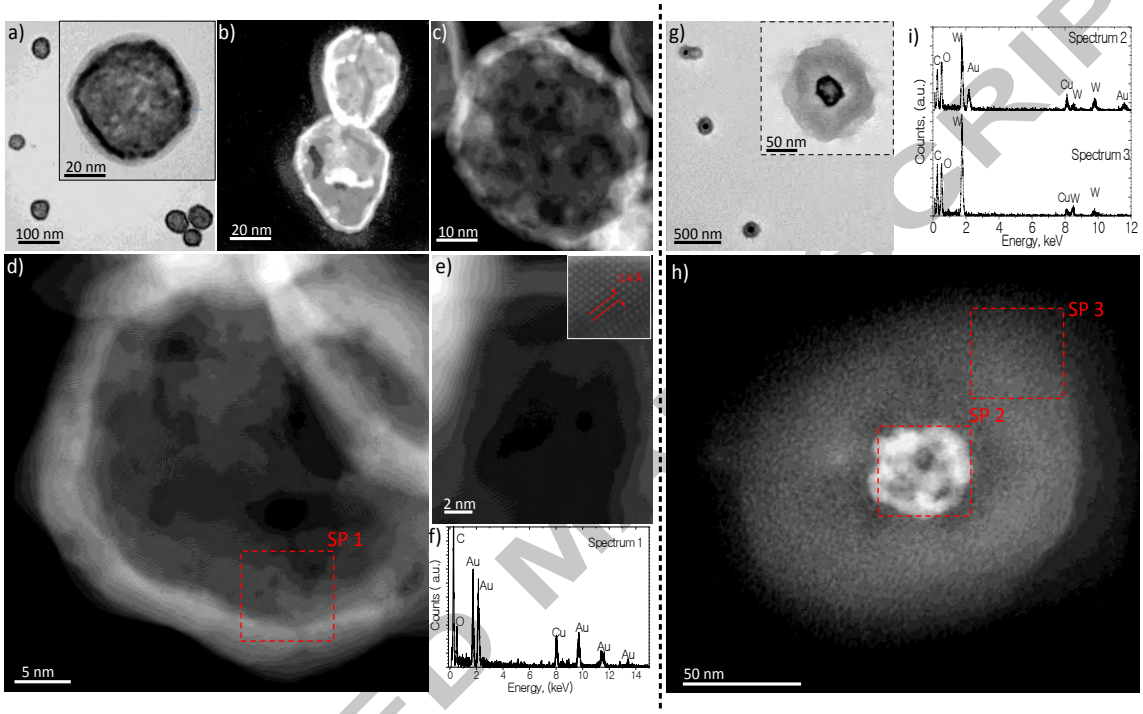

Fig. 2. Electron microscopy analysis of HGNPs@P(MEO_2MA-co-$OEGMA_{500}$) monolayer: (a) TEM images of a sample stained with a heavy metal phosphotungstic acid salt, used as a negative stain, to allow electronic observation of the polymer coating. Inset, a detailed TEM image to observe the polymer shell of aprox. 9 nm. (b-d) STEM-HAADF images of a stained sample to observe the location by Z – contrast of Au and W atoms. W atoms stained the polymeric shell. e) UHR-STEM-HAADF image to observe the polycrystalline structure of HGNPs. Inset is a detailed UHR-STEM-HAADF image of a pore in the HGNPs. (f) EDS analysis in the red-line area marked in d). Electron microscopy analysis of HGNPs@P(MEO_2MA-co-$OEGMA_{500}$) nanogel: (g) TEM Images of a sample stained with phosphotungstic acid salt. Inset, a detailed TEM image to observe the polymer shell of approx. 60 nm. (h) STEM-HAADF images of a stained sample to observe the location by Z –contrast of Au and W atoms. W atoms stained the polymeric shell. (i) EDS analysis in the red-line areas marked in h) to differentiate the core and shell chemical composition.

HGNPs@P(MEO_2MA-co-$OEGMA_{500}$) presented a maximum in the extinction spectrum at 814 nm as shown in Fig. 3a. The surface plasmon resonance (SPR) band of the gold nanoparticles was red-shifted 27 nm to the NIR region after functionalization with the polymer, due to changes in the shell dielectric constant and its thickness [58, 59]. Therefore the modified nanoparticles could be activated by 808nm-NIR laser irradiation to generate the heat required to activate the phase transition of the polymer

covalently coupled to their surface. The nanoparticle polymer content was determined by TGA in the temperature range from 30 to 600 ºC. Fig. 3b shows the weight loss of the NPs as a function of the temperature. The thermal decomposition of P(MEO_2MA-co-$OEGMA_{500}$) occurred between 200-420 ºC. The polymeric content corresponding to the weight loss in that temperature range was a 10 wt.%. The FTIR analysis corroborated the functionalization of the HGNPs with the polymer by the identification of the characteristic bands of the polymer (Fig. 3c), the broad band at 1109 cm^{-1} corresponds to the C-O-C stretching vibration and the 1720 cm^{-1} peak was ascribed to the stretching vibration of the C=O group of the polymer [55]. The stability of the resulting NPs was corroborated by demonstrating that the Zeta Potential value of the colloidal aqueous suspensions remained unvaried over several months of storage (results not shown) without showing any signs of agglomeration.

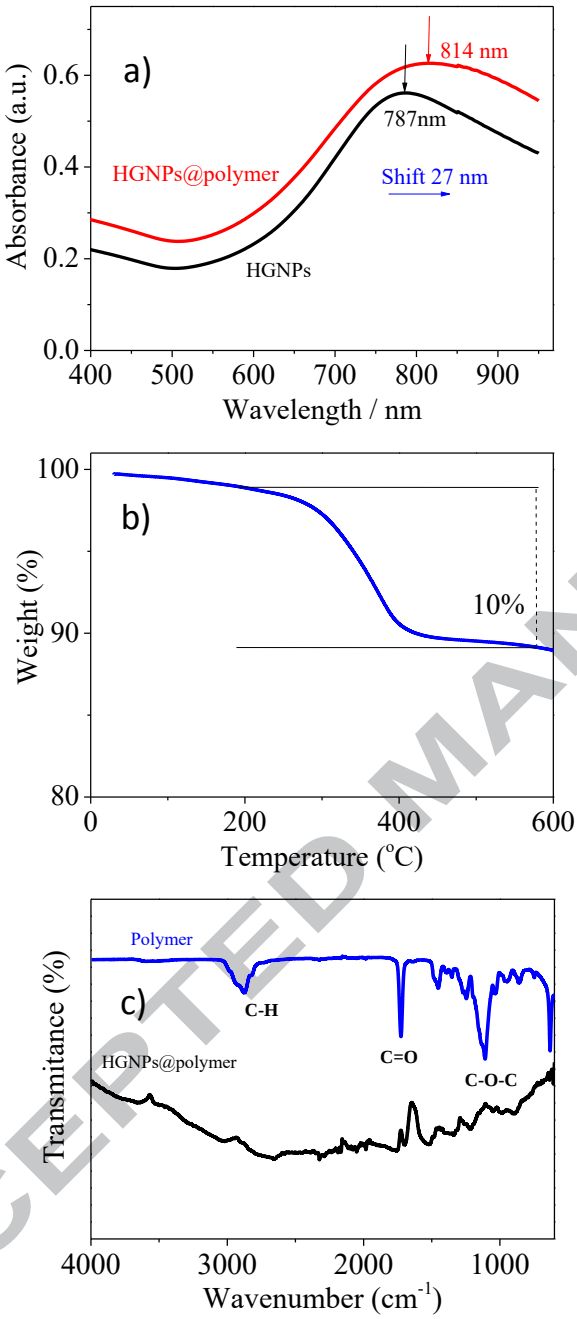

Fig. 3. (a) UV-Visible spectra of HGNP@P(MEO_2MA-co-$OEGMA_{500}$) and HGNPs. (b) Thermogravimetric analysis of HGNP@P(MEO_2MA-co-$OEGMA_{500}$) (c) FTIR of HGNP@P(MEO_2MA-co-$OEGMA_{500}$) and P(MEO_2MA-co-$OEGMA_{500}$) copolymer.

3.3. Bupivacaine loading and release

Nanoparticles were incubated with bupivacaine hydrochloride using a previously reported loading protocol [60], using a weight ratio 5/1 (nanoparticles/bupivacaine) to allow an efficient loading of the drug into the polymer shell. Bupivacaine hydrochloride was dissolved in distilled water to prepare a 0.32 mg/mL stock solution. 1 mL of this

bupivacaine solution was added into an Eppendorf tube® containing 1.6 mg of lyophilized HGNPs@P(MEO_2MA-co-$OEGMA_{500}$). The mixture was kept under stirring at room temperature for 4 h, and then the dispersion was centrifuged at 13000 rpm during 12 min to separate the nanoparticles, and carefully washed with 1 mL of additional water. The amount of bupivacaine loaded in the nanoparticles was determined indirectly determining the amount of drug remaining in the supernatant after loading, using UV-visible spectroscopy to quantify the bupivacaine at the detection wavelength of 262 nm. Drug loading was calculated by the following equation: $DL\% = \frac{Mass\ of\ drug\ in\ nanoparticles}{Total\ mass\ of\ nanoparticles}\ X\ 100$

Drug loading content determined spectrophotometrically was (3.0 ± 0.4) wt.%.

Zeta potential was used to study the nature of the interactions between the HGNPs@P(MEO_2MA-co-$OEGMA_{500}$) surface and bupivacaine. Bupivacaine hydrochloride is positively charged at neutral pH (pKa=8.1) and therefore, it can interact electrostatically with a negatively charged surface. Zeta potential measurements performed on HGNP@P(MEO_2MA-co-$OEGMA_{500}$) revealed a negative electrokinetic potential of -11.34 ± 1.10 mV in the nanoparticles (Fig. 4a), attributed to the sodium citrate used to stabilize the NPs and to the ethylene oxide groups of the P(MEO_2MA-co-$OEGMA_{500}$) polymer. HGNP@P(MEO_2MA-co-$OEGMA_{500}$) loaded with bupivacaine reduced their zeta potential to -4.2 ± 1.10 mV, pointing to a partial neutralization of the polymer negative charges by electrostatic interaction with bupivacaine. To evaluate the type of interaction nanoparticles loaded with bupivacaine were incubated in PBS buffer (as a competitive high ionic strength media) during 24 h, having an identical release profile than that achieved in deionized water. Therefore, through this assay we dismissed that binding of bupivacaine to NPs was driven exclusively by ionic interactions, so nonspecific absorption and hydrophobic interactions also contributed to drug encapsulation. Other authors pointed to both contributions using PNIPAM nanogels scavengers for bupivacaine [44].

In vitro release profiles of bupivacaine from HGNPs@P(MEO_2MA-co-$OEGMA_{500}$) dispersed in water were examined at physiological temperature, 37 ºC, which produces an expanded coil conformation of the polymer, below its LCST; and also at 45 ºC where the polymer would be organized in the collapsed globular conformation. Drug release induced by the reversible polymer phase transition was tested by monitoring the release under sequential heating pulses above (45 ºC) and

below (37 ºC) the LCST of the polymer. NPs loaded with bupivacaine were re-dispersed in 1 mL of water immediately after loading. The dispersions were then placed into a thermoshaker with mechanical agitation at 600 rpm at the temperature required (37 or 45 ºC) according to each assay. As shown in Fig. 4b, the drug release rate of HGNPs@P(MEO_2MA-co-$OEGMA_{500}$) was faster at 45 ºC than at physiological temperature (37 ºC). At high temperature (45 ºC), the cumulative drug released was considerably higher than that obtained at 37 ºC (Fig. 4b), probably due to a higher diffusion and favored desorption promoted by the increase in the temperature. The cumulative drug release data were fitted to mathematical models to elucidate the mechanism controlling bupivacaine delivery. The correlation coefficient (r) was determined from the linear regressions to zero order and Higuchi model. The release profile at 37ºC showed an r value of 0.976 and 0.998 for the fitting to zero order and Higuchi model, respectively. The release at 45 ºC also showed a better correlation to Higuchi model (Zero order r=0.989, Higuchi r=0.999). This indicates that the release process is controlled mainly by diffusion of the drug, as was shown previously in other nanoparticle-based systems [61]. When the temperature was varied above and below the LCST, in a pulsed release mode, the accumulated released drug from nanoparticles was quickly enhanced (Fig. 4b). The results clearly show that the pulsed release improves drug delivery on-demand, giving a much faster release rate. After 12 pulses, the cumulative diffusive release reached a 40% of the drug loaded, in less than 8 h, conversely bupivacaine release at 37 ºC took more than 160 h to obtain such cumulative drug release. Moreover, the doses of drug released were spatiotemporally controlled by the number of pulses supplied. The reason for these results is that the transition across the LCST causes the physical change of the polymer, to give a hydrophobic structure able to expel a fraction of the drug retained in the inner shell of the polymer. As it is shown in Fig. 4b, the amount of drug released followed a linear relationship with the number of pulses applied, due to a burst release as opposed to a diffusion-controlled release occurred at 37 ºC.

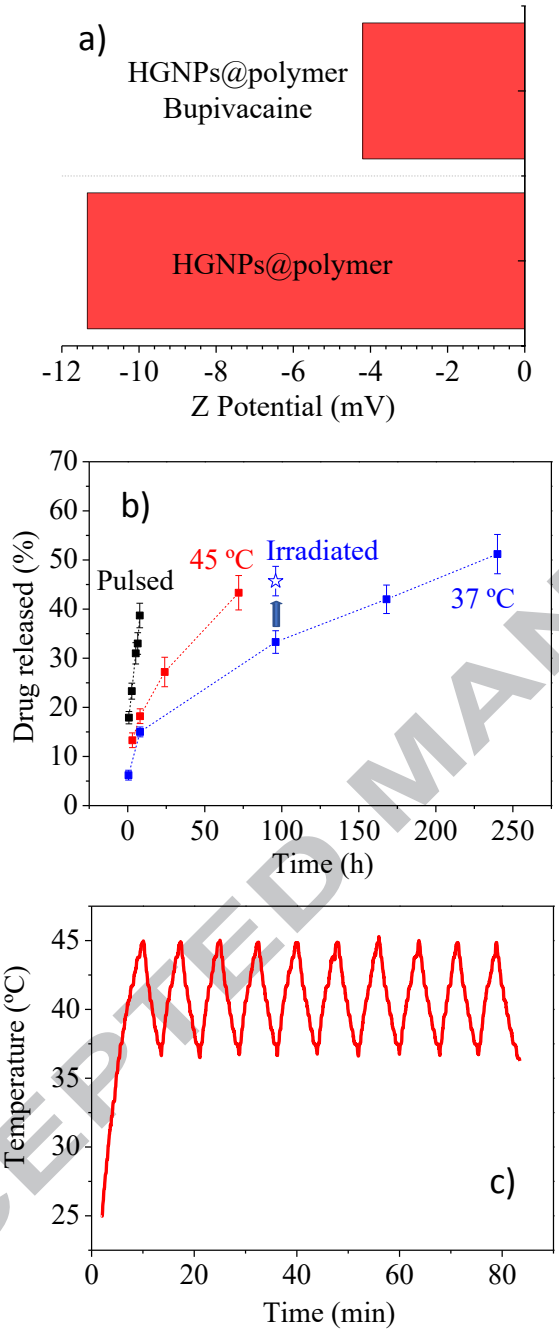

Fig. 4. (a) Zeta potential of HGNP@P(MEO_2MA-co-$OEGMA_{500}$) and HGNP@P(MEO_2MA-co-$OEGMA_{500}$) loaded with bupivacaine (b) Bupivacaine release profiles from HGNP@P(MEO_2MA-co-$OEGMA_{500}$) at different temperatures: 45 ºC, 37 ºC and pulses of temperature from 37 ºC to 45 ºC (the star corresponds to 10 cycles of irradiation). Percentages are displayed as mean ± SD (N = 3). (c) Heating curve of HGNP@P(MEO_2MA-co-$OEGMA_{500}$) dispersed in water with a concentration of 1.6 mg/mL and laser irradiance of 6.5 W/cm^2.

The photothermal response caused by HGNPs surface plasmon excitation upon 808 nm laser irradiation was also used to induce changes in the temperature from 37 ºC to 45 ºC. Fig. 4c shows the heating curves of 1.6 mg/mL nanoparticle dispersion in

water under a laser irradiance of 6.5 W/cm^2 (such high irradiance was used to obtain a fast response). After ten cycles, the temperature profiles showed no significant difference between the different irradiation cycles, indicating enhanced photostability of the HGNPs (Fig. 4c). Each pulse of temperature took around 7 minutes to complete, and after ten irradiation pulses in a sample incubated during 4 days at 37 ºC, the amount of drug released was determined spectrophotometrically. Controls made under the same conditions using water or PBS alone showed no heating after irradiation. Results in Fig. 4b (highlighted with an arrow), showed that the amount of drug released was a 12% higher when the photothermal stimulus was applied to trigger the release compared to the release obtained at 37 ºC. Thus, in case of a real application, a triggered on-demand release at specific time point can be achievable to provide with an extra of analgesia by using the nanoparticles here reported. We thus demonstrated that under NIR light irradiation the photothermal-induced reversible transition from coil to globule in the polymer can be used to provide with a stimulus-responsive triggered release of bupivacaine to improve pain management.

3.4. Cell viability assay

The cytocompatibility of the hybrid thermoresponsive materials synthesized was studied at different levels (cell metabolism, cell membrane and DNA) in four cell lines (human dermal fibroblasts, mMSCs, U251MG and human macrophages).

The treatment of the cell lines incubated with our particles (0.02-2 mg/mL) involved detrimental effects on cell metabolism and viability at the higher concentrations assayed as was determined by the Blue Cell Viability assay (Fig. 5). The increase in HGNPs@P(MEO_2MA-co-$OEGMA_{500}$) concentration (Fig. 5a) implied a decrease in viability higher than 50% at concentrations from 1 mg/mL in all the cell types studied, being less accentuated for U251MG. At the highest concentration assayed (2 mg/mL), the viability percentages obtained were between 31% (mMSCs) and 42% (U251MG). The addition of HGNPs@P(MEO_2MA-co-$OEGMA_{500}$) loaded with bupivacaine to the cell cultures (Fig. 5b) displayed similar viability percentages to those obtained in the case of the non-loaded particles, except for macrophages that exerted higher values. In this case, the percentages obtained at the higher concentration studied were between 33% (mMSCs) and 80% (macrophages). Taking into account these results and the recommendations of the ISO 10993-5 [62], 0.2 mg/mL was considered

the subcytotoxic concentration for further studies as this concentration displayed viability percentages higher than 70% in all the cell lines assayed and for both materials evaluated.

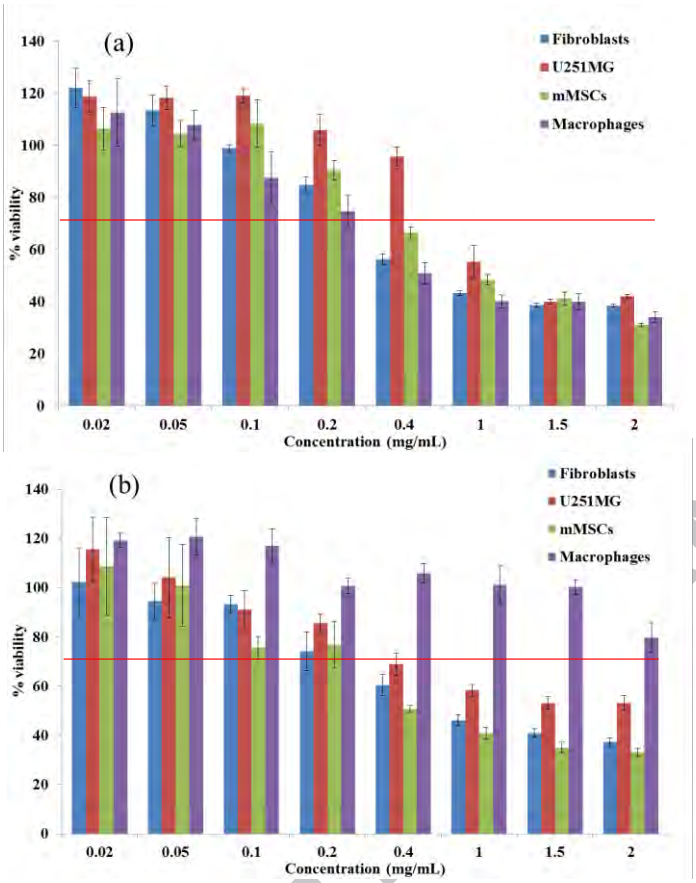

Fig. 5. Cell viability of HGNPs@P(MEO_2MA-co-$OEGMA_{500}$) (a) and HGNPs@P(MEO_2MA-co-$OEGMA_{500}$) loaded with bupivacaine (b), in the four cell lines assayed after 24 h. Percentages are displayed as mean ± SD (N = 5)

In order to obtain information about the effect of nanoparticles (HGNPs@P(MEO_2MA-co-$OEGMA_{500}$) on cell cycle progression and cell population distribution, we performed cell cycle analysis by flow cytometry. The results obtained from the cell cycle analysis are shown in Fig. S1. No significant nanoparticle-induced perturbation of the cell-cycle distribution were observed in THP1 macrophages and U251MG at subcytotoxic concentration (0.2 mg/mL), indicating nanoparticles do not deregulate the cell cycle and, therefore, they did not interfere with cell division or with cellular functions in these cell lines studied. In addition, no significant differences were observed in the degree of necrosis and both early and late apoptosis in THP1 macrophages and U251 MG cells after nanoparticle exposure (Table S1). In human dermal fibroblasts, an increase in G1 population accompanied by a marked decrease in G2 population compared to that observed for the control was measured after

nanoparticle treatment. However, S population was not affected as compared to that of the corresponding control. These data might suggest that nanoparticles could cause cell cycle arrest in G1 phase (Fig. S1). However, it is important to mention that no significant changes in the percentages of apoptotic and necrotic cells were observed after nanoparticle treatment at subcytotoxic concentration in this cell line (Table S1). In contrast to human dermal fibroblasts, in mMSCs, a marked increase in the percentage of cells in G1 phase with a concomitant decrease in G2 population were observed after 24 h of treatment with nanoparticles by comparison with control cells, indicating a possible cell cycle arrest at G2 phase (Fig. S1). In this case, nanoparticle exposure caused a slight increase in the percentage of early apoptotic cells (Table S1). These results indicated that the nanoparticle-induced cell cycle perturbations seem to be dependent on the cellular type. Thus, in fibroblasts, the addition of nanoparticles might retard cell proliferation without inducing cell death, probably acting as cytostatic agent. While in mMSCs, nanoparticles could suppress the progression of cell cycle at G2 phase. The data also suggest that only a small population of cells is undergoing cell death by apoptosis while higher percentage is alive. Furthermore, according to the recommendations indicated above of the American National Standard ISO 10993-5, HGNPs@P(MEO_2MA-co-$OEGMA_{500}$) nanoparticles showed appropriate biocompatibility for biomedical applications due to that their cytotoxic effect on cells was always lower than 30%.

To our knowledge this is the first report in the literature describing the functionalization of HGNPs with the thermoresponsive polymer disulfide-P(MEO_2MA-co-$OEGMA_{500}$) and, therefore, there is not previous data about the potential effects of these surface-functionalized nanoparticles on cell viability, cell cycle steps, apoptosis or necrosis. Due to the easy of functionalization of gold nanoparticles with thiolated chains, PEG is one of the most used biocompatible molecules for increasing the biocompatibility of gold nanomaterials. Several studies have described the influence of PEGylated gold nanoparticles on cell metabolism, cell cycle progression [63, 64] and in the induction of apoptosis [64] in both healthy and cancer cell lines. Regarding cell viability, these studies reported similar effects in the cell types assayed as those showed by our previously reported HGNPs, pointing to 0.1 mg/mL as the subcytotoxic concentration [63], while a concentration of 10 mM (2 mg/mL) PEG-AuNPs was clearly harmful for human chronic myeloid leukemia cell line K562 exerting viability percentages around 20% [64]. Also, a previous study showed that the interaction of

nanoparticles on cell cycle varied depending on both cell line and nanoparticle type. Thus, independent of their surface properties, PEGylated gold nanoparticles caused significant cell-cycle perturbation on several cancer cells without causing any apoptotic behavior [65] but, however, in healthy fibroblasts, the effect of PEGylated gold nanoparticles was dependent on PEG grafting density and hydrodynamic volume. Given that the effect of nanoparticles on cell cycle progression, apoptosis or necrosis may depend on the nature of the thermoresponsive polymer coating in the surface of gold nanoparticles. It is important to mention that OEGMA-based copolymers have been reported as non-cytotoxic at the highest concentration tested (i.e., 0.4 mg/mL) [46].

4. Conclusions

In summary, HGNPs surface functionalized with the thermoresponsive polymer disulfide-P(MEO_2MA-co-$OEGMA_{500}$) were fabricated and tested as drug delivery systems. The local anesthetic bupivacaine was loaded in the nanoparticles, obtaining a 3 wt.% drug loading. Drug-release results indicated that HGNPs@P(MEO_2MA-co-$OEGMA_{500}$) show thermoresponsive behavior and controllable release when treated above and below the LCST of the polymer. The spatiotemporal control of the drug release is achievable thanks to the polymer transition from coil to globule produced by photothermal heating. This feature is very attractive when using these NPs in biomedical applications such as on-demand drug delivery. In addition the biological studies highlighted their cytocompatibility at concentrations up to 0.2 mg/mL. Results demonstrated that NIR photoactivated HGNPs functionalized with the thermoresponsive P(MEO_2MA-co-$OEGMA_{500}$) could have great potential for on-demand controlled release of bupivacaine potentially used in the treatment of chronic pain.

ACKNOWLEDGMENTS

The authors thank financial support from the ERC Consolidator Grant program (ERC-2013-CoG-614715, NANOHEDONISM). CIBER-BBN is an initiative funded by the VI National R&D&i Plan 2008–2011 financed by the Instituto de Salud Carlos III with the assistance of the European Regional Development Fund. We also acknowledge Dr. Pilar Martin-Duque for gifting U251MG and mMSCs cell lines.

REFERENCES

[1] M. Moritz, M. Geszke-Moritz, The newest achievements in synthesis, immobilization and practical applications of antibacterial nanoparticles, Chem. Eng. Sci., 228 (2013) 596-613.
[2] P. Thoniyot, M.J. Tan, A.A. Karim, D.J. Young, X.J. Loh, Nanoparticle–Hydrogel Composites: Concept, Design, and Applications of These Promising, Multi-Functional Materials, Adv. Sci., 2 (2015) 1400010-n/a.
[3] K.A. Juby, C. Dwivedi, M. Kumar, S. Kota, H.S. Misra, P.N. Bajaj, Silver nanoparticle-loaded PVA/gum acacia hydrogel: Synthesis, characterization and antibacterial study, Carbohydr. Polym., 89 (2012) 906-913.
[4] P.C. Papaphilippou, A. Pourgouris, O. Marinica, A. Taculescu, G.I. Athanasopoulos, L. Vekas, T. Krasia-Christoforou, Fabrication and characterization of superparamagnetic and thermoresponsive hydrogels based on oleic-acid-coated Fe3O4 nanoparticles, hexa(ethylene glycol) methyl ether methacrylate and 2-(acetoacetoxy)ethyl methacrylate, J. Magn. Magn. Mater., 323 (2011) 557-563.
[5] O. Korotych, Y. Samchenko, I. Boldeskul, Z. Ulberg, N. Zholobak, L. Sukhodub, N-isopropylacrylamide-based fine-dispersed thermosensitive ferrogels obtained via in-situ technique, Mater. Sci. Eng. C 33 (2013) 892-900.
[6] Q. Wang, R. Hou, Y. Cheng, J. Fu, Super-tough double-network hydrogels reinforced by covalently compositing with silica-nanoparticles, Soft Matter, 8 (2012) 6048-6056.
[7] X. Hu, X. Hao, Y. Wu, J. Zhang, X. Zhang, P.C. Wang, G. Zou, X.- . Liang, Multifunctional hybrid silica nanoparticles for controlled doxorubicin loading and release with thermal and p dual response, J. Mater. Chem. B 1(2013) 1109-1118.
[8] G.S. Alvarez, C. Helary, A.M. Mebert, X. Wang, T. Coradin, M.F. Desimone, Antibiotic-loaded silica nanoparticle-collagen composite hydrogels with prolonged antimicrobial activity for wound infection prevention, J. Mater. Chem. B 2(2014) 4660-4670.
[9] S.K. Samanta, A. Pal, S. Bhattacharya, C.N.R. Rao, Carbon nanotube reinforced supramolecular gels with electrically conducting, viscoelastic and near-infrared sensitive properties, J. Mater. Chem, 20 (2010) 6881-6890.
[10] C.-W. Lo, D. Zhu, H. Jiang, An infrared-light responsive graphene-oxide incorporated poly(N-isopropylacrylamide) hydrogel nanocomposite, Soft Matter, 7 (2011) 5604-5609.
[11] Y. Brudno, D.J. Mooney, On-demand drug delivery from local depots, J. Control. Release 219 (2015) 8-17.
[12] J. Zhang, L. Wu, F. Meng, Z. Wang, C. Deng, H. Liu, Z. Zhong, pH and Reduction Dual-Bioresponsive Polymersomes for Efficient Intracellular Protein Delivery, Langmuir, 28 (2012) 2056-2065.
[13] Y. Li, W. Xiao, K. Xiao, L. Berti, J. Luo, H.P. Tseng, G. Fung, K.S. Lam, Well-Defined, Reversible Boronate Crosslinked Nanocarriers for Targeted Drug Delivery in Response to Acidic pH Values and cis-Diols, Angew. Chem. Int. Ed., 51 (2012) 2864-2869.
[14] W. Chen, Y. Cheng, B. Wang, Dual-Responsive Boronate Crosslinked Micelles for Targeted Drug Delivery, Angew. Chem. Int. Ed., 51 (2012) 5293-5295.
[15] A. Hervault, A.E. Dunn, M. Lim, C. Boyer, D. Mott, S. Maenosono, N.T.K. Thanh, Doxorubicin loaded dual pH- and thermo-responsive magnetic nanocarrier for

combined magnetic hyperthermia and targeted controlled drug delivery applications, Nanoscale, 8 (2016) 12152-12161.
1 . Shen, . Ma, S. u , . i, Smart Multifunctional Magnetic a noparticle- ased Drug Delivery System for ancer Thermo- hemotherapy and Intracellular Imaging, ACS Appl. Mater. Interfaces 8(2016) 24502-24508.
[17] Q. Ban, T. Bai, X. Duan, J. Kong, Noninvasive photothermal cancer therapy nanoplatforms via integrating nanomaterials and functional polymers, Biomater. Sci, 5 (2017) 190-210.
[18] M. Ghorbani, H. Hamishehkar, N. Arsalani, A.A. Entezami, A novel dual-responsive core-crosslin e d magnetic-gold nanogel for triggered drug release, Mater. Sci. Eng. C 68 (2016) 436-444.
[19] G. Vancoillie, D. Frank, R. Hoogenboom, Thermoresponsive poly(oligo ethylene glycol acrylates), Prog. Polym. Sci., 39 (2014) 1074-1095.
[20] H. García-Juan, A. o gales, E. lasco, . . Martínez, I. Šics, T.A. Ezquerra, M. Piñol, L. Oriol, Self-assembly of thermo and light responsive amphiphilic linear dendritic block copolymers, Eur. Polym. J., 81 (2016) 621-633.
[21] Z. Hu, T. Cai, C. Chi, Thermoresponsive oligo(ethylene glycol)-methacrylate-based polymers and microgels, Soft Matter, 6 (2010) 2115-2123.
[22] B.P. Timko, M. Arruebo, S.A. Shankarappa, J.B. McAlvin, O.S. Okonkwo, B. Mizrahi, C.F. Stefanescu, L. Gomez, J. Zhu, A. Zhu, J. Santamaria, R. Langer, D.S. Kohane, Near-infrared–actuated devices for remotely controlled drug delivery, Proc. Natl. Acad. Sci. U.S.A., 111 (2014) 1349-1354.
[23] E. Hemmer, M. Quintanilla, F. Légaré, F. Vetrone, Temperature-Induced Energy Transfer in Dye-Conjugated Upconverting Nanoparticles: A New Candidate for Nanothermometry, Chem. Mater., 27 (2015) 235-244.
[24] S. Schmidt, M. Zeiser, T. Hellweg, C. Duschl, A. Fery, H. Möhwald, Adhesion and Mechanical Properties of PNIPAM Microgel Films and Their Potential Use as Switchable Cell Culture Substrates, Adv. Funct. Mater 20 (2010) 3235-3243.
[25] T. Trongsatitkul, B.M. Budhlall, Multicore–Shell PNIPAm-co-PEGMa Microcapsules for Cell Encapsulation, Langmuir, 27 (2011) 13468-13480.
[26] S. Ohya, Y. Nakayama, T. Matsuda, Thermoresponsive Artificial Extracellular Matrix for Tissue Engineering: yaluronic Acid ioconjugated with Poly(-isopropylacrylamide) Grafts, Biomacromolecules, 2 (2001) 856-863.
[27] H. Vihola, A. Laukkanen, L. Valtola, H. Tenhu, J. Hirvonen, Cytotoxicity of thermosensitive polymers poly(N-isopropylacrylamide), poly(N-vinylcaprolactam) and amphiphilically modified poly(N-vinylcaprolactam), Biomaterials, 26 (2005) 3055-3064.
[28] J.-F. Lutz, Ö. Akdemir, A. Hoth, Point by Point Comparison of Two Thermosensitive Polymers Exhibiting a Similar L ST: Is the Age of Poly(I PAM) Over?, JACS, 128 (2006) 13046-13047.
[29] M.A. Cooperstein, H.E. Canavan, Assessment of cytotoxicity of (N-isopropyl acrylamide) and Poly(N-isopropyl acrylamide)-coated surfaces, Biointerphases, 8 (2013) 19.
[30] J.-F. Lutz, A. Hoth, Preparation of Ideal PEG Analogues with a Tunable Thermosensitivity by Controlled Radical Copolymerization of 2-(2-Methoxyethoxy)ethyl Methacrylate and Oligo(ethylene glycol) Methacrylate, Macromolecules, 39 (2006) 893-896.
[31] A. Shiotani, T. Mori, T. Niidome, Y. Niidome, Y. Katayama, Stable Incorporation of Gold Nanorods into N-Isopropylacrylamide Hydrogels and Their Rapid Shrinkage Induced by Near-Infrared Laser Irradiation, Langmuir, 23 (2007) 4012-4018.

[32] A.Y. Rwei, B.Y. Wang, T. Ji, C. Zhan, D.S. Kohane, Enhanced Triggering of Local Anesthetic Particles by Photosensitization and Photothermal Effect Using a Common Wavelength, Nano Lett., (2017).
[33] R. Cheng, F. Meng, C. Deng, H.-A. Klok, Z. Zhong, Dual and multi-stimuli responsive polymeric nanoparticles for programmed site-specific drug delivery, Biomaterials, 34 (2013) 3647-3657.
[34] Y. Li, J. Zhang, Y. Xu, Y. Han, B. Jiang, L. Huang, H. Zhu, Y. Xu, W. Yang, C. Qin, The Histopathological Investigation of Red and Blue Light Emitting Diode on Treating Skin Wounds in Japanese Big-Ear White Rabbit, PLoS One, 11 (2016) e0157898.
[35] Z. Zhang, J. Wang, X. Nie, T. Wen, Y. Ji, X. Wu, Y. Zhao, C. Chen, Near Infrared Laser-Induced Targeted Cancer Therapy Using Thermoresponsive Polymer Encapsulated Gold Nanorods, JACS, 136 (2014) 7317-7326.
[36] J. Park, J. Park, E.J. Ju, S.S. Park, J. Choi, J.H. Lee, K.J. Lee, S.H. Shin, E.J. Ko, I. Park, C. Kim, J.J. Hwang, J.S. Lee, S.Y. Song, S.-Y. Jeong, E.K. Choi, Multifunctional hollow gold nanoparticles designed for triple combination therapy and T imaging, J. Control. Release, 207 (2015) 77-85.
[37] G.J. Hobbs, F.L. Roberts, Epidural infusion of bupivacaine and diamorphine for postoperative analgesia, Anaesthesia, 47 (1992) 58-62.
[38] A. Lee, D. Simpson, A. Whitfield, D.B. Scott, Postoperative analgesia by continuous extradural infusion of bupivacaine and diamorphine Br. J. Anaesth, 60 (1988) 845-850.
[39] A.C. Norton, A.G. Davis, R.J. Spicer, Lignocaine 2% with adrenaline for epidural Caesarean section, Anaesthesia, 43 (1988) 844-849.
[40] C.M. Essink-Tjebbes, D.M. Burger, M. Beelen, E.W. Wuis, Y.A. Hekster, Long- term stability of morphine and bupivacaine mixture for spinal use, Pharm. World Sci., 21 (1999) 144-146.
[41] J. Robinson, R. Fernando, W.Y.S. Sun Wai, F. Reynolds, Chemical stability of bupivacaine, lidocaine and epinephrine in pH-adjusted solutions, Anaesthesia, 55 (2000) 853-858.
[42] V.V. Dinh, Y.-S. Suh, H.-K. Yang, Y.T. Lim, Spatiotemporal Programing for the On-Demand elease of upivacaine ased on an Injectable omposite ydrogel, J. Pharm. Sci, 105 (2016) 3634-3644.
[43] F. Taraballi, S. Minardi, B. Corradetti, I.K. Yazdi, M.A. Balliano, J.L. Van Eps, M. Allegri, E. Tasciotti, Potential Avoidance of Adverse Analgesic Effects Using a iologically “Smart” ydrogel apable of ontrolled upivacaine elease, . Pharm. Sci, 103 (2014) 3724-3732.
[44] T. Hoare, D. Sivakumaran, C.F. Stefanescu, M.W. Lawlor, D.S. Kohane, Nanogel scavengers for drugs: Local anesthetic uptake by thermoresponsive nanogels, Acta Biomater., 8 (2012) 1450-1458.
[45] T. Hoare, S. Young, M.W. Lawlor, D.S. Kohane, Thermoresponsive nanogels for prolonged duration local anesthesia, Acta Biomater., 8 (2012) 3596-3605.
[46] T. Alejo, M. Prieto, H. García-Juan, V. Andreu, G. Mendoza, V. Sebastian, M. Arruebo, A facile method for the controlled polymerization of biocompatible and thermoresponsive oligo(ethylene glycol) methyl ether methacrylate copolymers, Polym. J., (2017) DOI 10.1038/s41428-017-0004-8.
[47] S. Preciado-Flores, D. Wang, D.A. Wheeler, R. Newhouse, J.K. Hensel, A. Schwartzberg, L. Wang, J. Zhu, M. Barboza-Flores, J.Z. Zhang, Highly reproducible synthesis of hollow gold nanospheres with near infrared surface plasmon absorption using PVP as stabilizing agent, J. Mater. Chem., 21 (2011) 2344-2350.

[48] L. Gomez, V. Sebastian, S. Irusta, A. Ibarra, M. Arruebo, J. Santamaria, Scaled-up production of plasmonic nanoparticles using microfluidics: from metal precursors to functionalized and sterilized nanoparticles, Lab Chip, 14 (2014) 325-332.
[49] F. Gambinossi, M. Chanana, S.E. Mylon, J.K. Ferri, Programming nanoparticle aggregation kinetics with poly(MeO2MA-co-OEGMA) copolymers, Soft Matter, 9 (2013) 11046-11053.
[50] E.W. Edwards, M. Chanana, D. Wang, H. Möhwald, Stimuli-Responsive Reversible Transport of Nanoparticles Across Water/Oil Interfaces, Angew. Chem., 47 (2008) 320-323.
[51] N. Guarrotxena, I. Quijada-Garrido, Optical and Swelling Stimuli-Response of Functional Hybrid Nanogels: Feasible Route to Achieve Tunable Smart Core@Shell Plasmonic@Polymer Nanomaterials, Chem. Mater., 28 (2016) 1402-1412.
[52] V. Aseyev, H. Tenhu, F.M. Winnik, Non-ionic Thermoresponsive Polymers in Water, in: A.H.E. Müller, O. Borisov (Eds.) Self Organized Nanostructures of Amphiphilic Block Copolymers II, Springer Berlin Heidelberg, Berlin, Heidelberg, 2010, pp. 29-89.
[53] J.-F. Lutz, K. Weichenhan, Ö. Akdemir, A. Hoth, About the Phase Transitions in Aqueous Solutions of Thermoresponsive Copolymers and Hydrogels Based on 2-(2-methoxyethoxy)ethyl Methacrylate and Oligo(ethylene glycol) Methacrylate, Macromolecules, 40 (2007) 2503-2508.
[54] L. Li, B. Lu, J. Wu, Q. Fan, X. Guo, Z. Liu, Synthesis and self-assembly behavior of thermo-responsive star-shaped POSS-(PCL-P(MEO2MA-co-PEGMA))16 inorganic/organic hybrid block copolymers with tunable lower critical solution temperature, New J. Chem, 40 (2016) 4761-4768.
[55] J.M. García-García, M. Liras, I. Quijada-Garrido, A. Gallardo, R. París, Swelling control in thermo-responsive hydrogels based on 2-(2-methoxyethoxy)ethyl methacrylate by crosslinking and copolymerization with N-isopropylacrylamide, Polym. J., 43 (2011) 887.
[56] C. Louis, O. Pluchery, Gold Nanoparticles for Physics, Chemistry and Biology, Imperial College Press, London, 2012.
[57] E. Luque-Michel, A. Larrea, C. Lahuerta, V. Sebastian, E. Imbuluzqueta, M. Arruebo, M.J. Blanco-Prieto, J. Santamaria, A simple approach to obtain hybrid Au-loaded polymeric nanoparticles with a tunable metal load, Nanoscale, 8 (2016) 6495-6506.
[58] M. Karg, S. Jaber, T. Hellweg, P. Mulvaney, Surface Plasmon Spectroscopy of Gold−Poly-N-isopropylacrylamide ore−Shell Particles, Langmuir, 27 (2011) 820-827.
[59] M. Dulle, S. Jaber, S. Rosenfeldt, A. Radulescu, S. Forster, P. Mulvaney, M. Karg, Plasmonic gold-poly(N-isopropylacrylamide) core-shell colloids with homogeneous density profiles: a small angle scattering study, Phys. Chem. Chem. Phys., 17 (2015) 1354-1367.
[60] I. Venditti, L. Fontana, I. Fratoddi, C. Battocchio, C. Cametti, S. Sennato, F. Mura, F. Sciubba, M. Delfini, M.V. Russo, Direct interaction of hydrophilic gold nanoparticles with dexamethasone drug: Loading and release study, J. Colloid Interface Sci 418 (2014) 52-60.
[61] L. Espanol, A. Larrea, V. Andreu, G. Mendoza, M. Arruebo, V. Sebastian, M.S. Aurora-Prado, E.R.M. Kedor-Hackmann, M.I.R.M. Santoro, J. Santamaria, Dual encapsulation of hydrophobic and hydrophilic drugs in PLGA nanoparticles by a single-step method: drug delivery and cytotoxicity assays, RSC Adv., 6 (2016) 111060-111069.

[62] ISO 10993- 5:2009 - Biological evaluation of medical devices. Part 5: Tests for in vitro cytotoxicity. http://www.iso.org/iso/catalogue_detail.htm?csnumber=36406. [Accessed: 30- Dec- 2017]
[63] M.d.M. Encabo-Berzosa, M. Sancho-Albero, A. Crespo, V. Andreu, V. Sebastian, S. Irusta, M. Arruebo, P. Martin-Duque, J. Santamaria, The effect of PEGylated hollow gold nanoparticles on stem cell migration: potential application in tissue regeneration, Nanoscale, 9 (2017) 9848-9858.
[64] Y.-C. Huang, Y.-C. Yang, K.-C. Yang, H.-R. Shieh, T.-Y. Wang, Y. Hwu, Y.-J. Chen, Pegylated Gold Nanoparticles Induce Apoptosis in Human Chronic Myeloid Leukemia Cells, BioMed Research International, 2014 (2014) 9.
[65] M. Uz, V. Bulmus, S. Alsoy Altinkaya, Effect of PEG Grafting Density and Hydrodynamic Volume on Gold Nanoparticle–Cell Interactions: An Investigation on Cell Cycle, Apoptosis, and DNA Damage, Langmuir, 32 (2016) 5997-6009.

Graphical abstract